

COMMUNICATION

Enzyme-Mediated Dual-Targeted-Assembly Achieves Synergetic Anticancer Effect

Received 00th January 20xx,
Accepted 00th January 20xx

Dingze Mang,^{a,†} Shijin Zhang,^{a,†} Xia Wu,^a Xunwu Hu,^a Toshiaki Mochizuki,^b Guanying Li^a and Ye ZHANG^{*,a}

DOI: 10.1039/x0xx00000x

We designed and synthesized homochiral-peptide-based boron diketonate complexes. Co-administration of the two stereoisomers on cancer cells let to molecular assembly targeting both the plasma membrane and the lysosomes mediated via membrane-bonded enzymes. The dual-targeted-assembly generates synergetic anticancer effect with amplified cancer spheroid toxicity and enhanced inhibition efficacy on cancer cell migration.

Combination treatments are the current trend leading anti-cancer drug research and development. Compared to single drugs, drug combinations, with multiple targets, offer a means to simplify complex treatment regimes with a better chance of affecting the equilibrium of cellular networks to cure complex diseases.¹ Greater efficacy of combination treatments using particular small molecule drug combinations compared with higher dose single drugs has been identified.³ Although molecular assembly (MA) has been applied in the development of combination therapy, nano-encapsulations as carriers for the delivery of multiple small molecule drugs were the only reported applications.^{4,5} Plasma-membrane-targeted MA has been established progressively as promising drug design to induce programmed cancer cell death.^{6,7} Considering the initiation or amplification effects of lysosomal membrane permeabilization (LMP)⁸ on the cell death program,^{9,10} we intend to incorporate molecular assemblies of plasma membrane targeting with lysosome targeting for a synchronized anti-cancer effect.¹¹ As shown in Figure 1, co-administration of two precursor molecules leads to plasma membrane and lysosome dual-targeted molecular assemblies¹² mediated via membrane enzyme—placental alkaline phosphatase (PLAP)¹³ that is highly expressed in cervical tumor as cancer biomarker. The programmed cancer cell death is promoted and amplified efficacy is achieved.

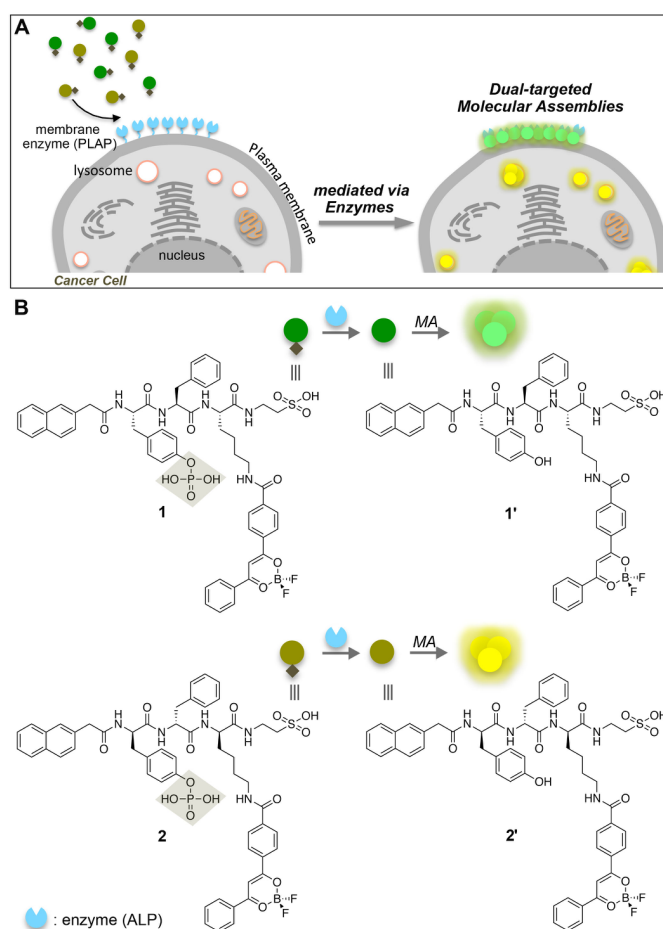


Figure 1. (A) Schematic illustration of enzyme-mediated dual-targeted MAs in vitro. Mediated via enzymes highly expressed on the plasma membrane of cancer cells, co-administration of molecular precursors induces MA targeting of both the plasma membrane and lysosomes. (B) Chemical structures of precursor molecules **1** and **2**. Hydrolysed by ALP, **1** and **2** convert to **1'** and **2'**, respectively, initiating MA with AIE.

To construct multiple targeting MAs, synthetic peptides with impressive chiral recognition abilities¹⁴ are applied as main building blocks of precursor molecules for protein-guided MA with high precisions in vitro.¹⁵ A pair of homochiral peptides, Naphthalene-*p*-Tyr-Phe-Lys-tyrosine and Naphthalene-*p*-tyr-phe-lys-

^a Bioinspired Soft Matter Unit, Okinawa Institute of Science and Technology Graduate University, 1919-1 Tancha, Onna-son, Okinawa, 904-0495, Japan.

^b Imaging Section, Okinawa Institute of Science and Technology Graduate University, 1919-1 Tancha, Onna-son, Okinawa, 904-0495, Japan.

[†] These authors contribute equally to this work.

Electronic Supplementary Information ² available: See DOI: 10.1039/x0xx00000x

taurine, coupled with the aggregation-induced emission (AIE) enhancement building block–boron diketone¹⁶ on the side chain of lysine are synthesized to obtain a pair of stereoisomers **1** and **2** (Figure 1). Via alkaline phosphatase (ALP)-catalysed hydrolysis, **1** and **2** can convert to assembly building blocks **1'** and **2'**, respectively. With fluorescence induced by MA, we will be able to track the localization of MA in vitro.

Under UV light, phosphate buffered saline (PBS) solutions of **1** or **2** were lit up by emitting blue light following the addition of ALP (Figure 2A). After hydrolysis is completed (confirmed by LCMS), we characterized the MA using transmission electron microscopy (TEM) and circular dichroism (CD) spectroscopy. Compared to PBS solutions of **1** or **2** at the concentration of 100 μM without MA, we found uniform nanofibers with around 6 nm in width tangling into dense networks after ALP-catalysed hydrolysis (Figure 2B), and short strands of nanothread with much lower density (Figure 2C), respectively. The CD spectrum of **1** in PBS buffer shows a negative peak at 210 nm and a positive peak at 220 nm (Figure S1). The CD spectrum of **2** in PBS buffer is the specular image of **1**, which is consistent with the chirality of both molecules' peptide building blocks.¹⁷ After ALP-catalysed hydrolysis, the CD spectra of the two solutions show a negative peak and a positive peak centred at 231 nm, respectively, indicating that the chirality of the peptide building blocks is transferred supramolecularly to the assembled nanostructures.¹⁸

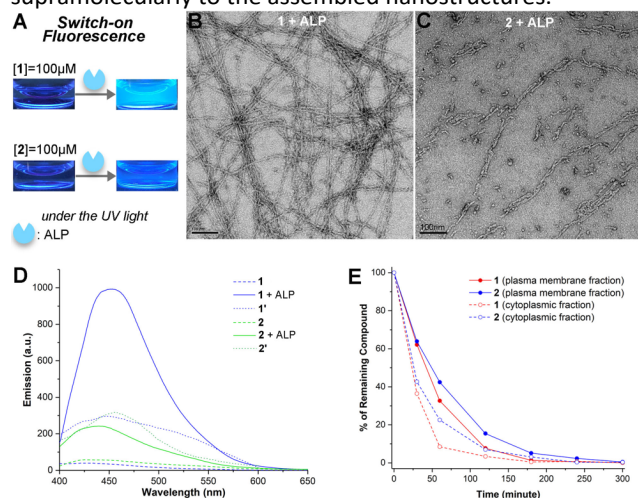


Figure 2. (A) Optical images of molecules **1** and **2** before and after the ALP catalysed hydrolysis in PBS buffer at the concentration of 100 μM under UV light. TEM images of **1** (B) and **2** (C) in PBS buffer at the concentration of 100 μM by the end of their ALP catalysed hydrolysis. Scale bar is 100 nm. (D) Emission spectra of **1** and **2** before (labelled as **1**, **2**) and after (labelled as **1** + ALP, **2** + ALP) the ALP catalysed hydrolysis, **1'** and **2'** in PBS buffer at the concentration of 100 μM excited at 350 nm. (E) Kinetic profiles of enzyme catalysed hydrolysis of **1** and **2** in plasma membrane fraction and cytosolic fraction of HeLa cells at 37 $^{\circ}\text{C}$.

The difference in MAs is also reflected by their AIE intensities (Figure 2D). Excited at 350 nm (Figure S2), PBS solutions of **1** or **2** show no MAs. Thus, both solutions exhibit weak emissions around 420 nm. Because of the same chemical structures, **1'** and **2'** in PBS solutions show enhanced fluorescence with similar intensities by forming identical uniform nanofibers via direct MA (Figure S3). Mediated via enzyme-catalysed

hydrolysis, the induced MA of different chiral molecules promotes fluorescent intensities to different levels. For example, after the addition of ALP, the fluorescence intensity of PBS solution of **1** is 5 times higher than the PBS solution of **2**, which is consistent with their enzyme-induced MA performance (Figure 2B and 2C). The results suggest that enzyme-mediation can differentiate chiral molecules **1** and **2** into divergent MAs leading to distinct nanostructures different from direct assembly of **1'** and **2'**.

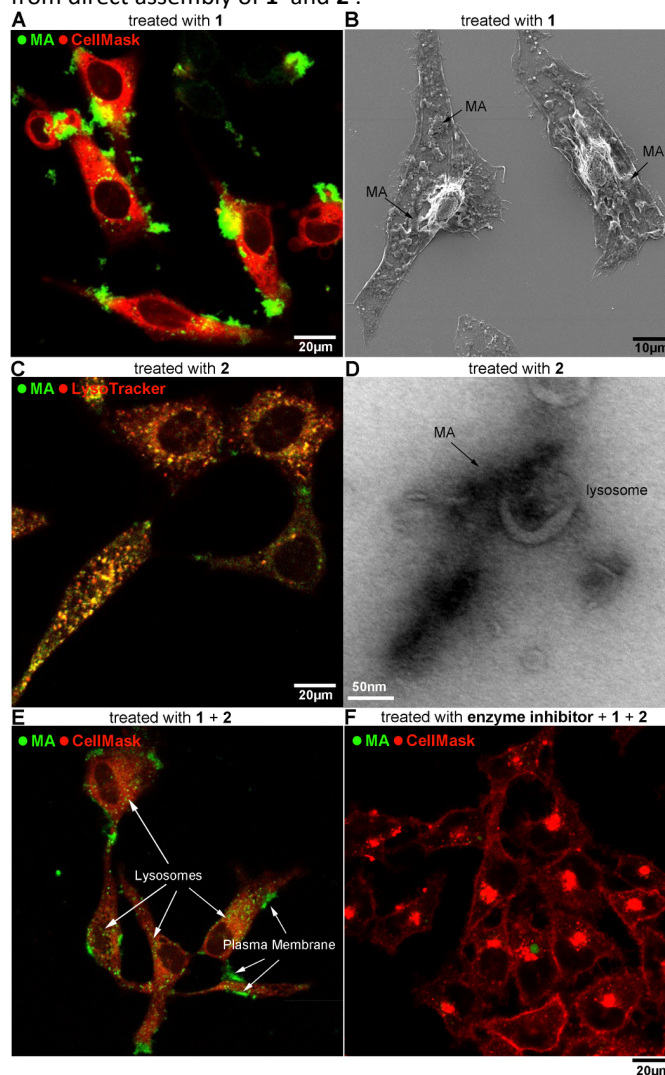


Figure 3. (A) Fluorescent image of HeLa cells incubated with **1** (100 μM , 12 h) and co-stained with CellMask Red. (B) SEM image of HeLa cells incubated with **1** (100 μM , 12 h). (C) Fluorescent image of HeLa cells incubated with **2** (100 μM , 12 h) and co-stained with LysoTracker Red. (D) TEM image of lysosomes isolated from HeLa cells incubated with **2** (100 μM , 12 h). Fluorescent image of HeLa cells incubated with the mixture of **1** and **2** (1:1, total concentration 100 μM , 12 h) without (E) and with (F) PLAP inhibition, and co-stained with CellMask Red.

To characterize the hydrolysis kinetics of both molecules **1** and **2** in vitro, we monitored their composition changes in isolated plasma membrane fraction and cytosolic fraction of HeLa cells at 37 $^{\circ}\text{C}$ (Figure 2E and S4). In plasma membrane fraction, **1** was hydrolysed faster than **2**, and **2** was hydrolysed faster in cytosolic fraction than in plasma membrane fraction. Combined with the higher density of stable nanostructures

induced by enzyme-catalysed hydrolysis of **1**, it has a better chance to induce MA on plasma membrane before entering into cells than **2**.

To examine the enzyme-mediated MA in vitro, we cultured HeLa cells that highly express PLAP on the plasma membrane for cell imaging. After 12-hour incubation with **1**, fluorescent patches are observed on the plasma membrane (Figure 3A). Scanning electron microscopy imaging confirmed the formation of MAs on HeLa cell membrane (Figure 3B). After 12-hour incubation with **2**, fluorescent signals are observed inside the cells and co-localize with lysosomes (Figure 3C). The TEM image of isolated lysosomes exhibits nano-aggregates suggesting the formation of MAs in lysosomes (Figure 3D and S5). Co-administration of **1** and **2** at 1:1 ratio in HeLa cell culture for 12 hours induced fluorescent signals both on plasma membrane and in lysosomes indicating the success of a dual-targeted MA (Figure 3E). Inhibiting the PLAP activity,¹⁹ co-administration of **1** and **2** did not induce MA on the plasma membrane or in the cytoplasm of HeLa cells suggesting that the PLAP is essential in enzyme-mediated dual-targeted MA.

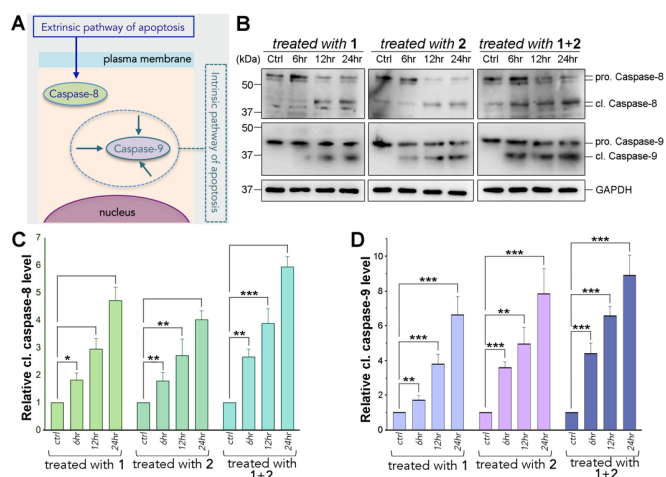


Figure 4. (A) Schematic illustration of simplified extrinsic and intrinsic apoptotic pathways. (B) Western blotting for Caspase-8 and Caspase-9 expressed in HeLa cells under the treatment of **1**, **2** and mixture of **1** and **2** at 1:1 ratio. GAPDH is a loading control. Time-dependent expression profiles of cleaved forms of caspase-8 (cl. Caspase-8) (C) and cleaved forms of caspase-9 (cl. Caspase-9) (D) in HeLa cells under the treatment of **1**, **2** and mixture of **1** and **2** at 1:1 ratio. Results are means \pm S.D. of three independent experiments. *, $p < 0.05$; **, $p < 0.01$; ***, $p < 0.001$.

Single-administration and co-administration of **1** and **2** on HeLa cells both triggered apoptotic pathways (Figure S6). Most apoptotic programs fall into either the extrinsic or intrinsic category triggered by extracellular cues or intracellular stimuli. The extrinsic pathway is mediated by caspase-8 while the intrinsic pathway is mediated by caspase-9 (Figure 4A).²⁰ The activities of both caspases were evaluated by western blotting (Figure 4B). As shown in Figure 4C, after 24-hour incubation, HeLa cells under the treatment of **1** showed 20% higher expression level of cleaved caspase-8 than under the treatment of **2**. In Figure 4D, since 6-hour incubation, HeLa cells under the treatment of **2** showed obvious higher expression level of cleaved caspase-9 than under the treatment of **1**. The activation of both caspases induced by two

molecules is consistent with their subcellular targets. HeLa cells under the co-treatment of **1** and **2** show higher expression levels of both cleaved caspase-8 and cleaved caspase-9 than both single administrations of two molecules. For example, 6-hour co-administration of **1** and **2** induce HeLa cells express similar amount of cleaved caspase-8 and cleaved caspase-9 as 12-hour single-administration with the same total concentration. The comparisons indicated that dual-targeted MA induced by co-administration of **1** and **2** promotes the cell death program with amplified apoptotic effect.

To evaluate the anti-cancer efficacy of dual-targeted MA, we examined the HeLa cell viability under the co-administration of **1** and **2** compared to their single-administrations. In 2D HeLa cell culture, D-version peptide molecule **2** showed higher toxicity than **1**,²¹ while co-administration of **1** and **2** exhibited similar toxicity as single-administration of **2** (Figure S7A). Co-administration exhibited enhanced anti-cancer efficacy in 3D cell cultures compare to single-administrations. As shown in Figure 5A at total concentration of 50 μ M, co-administration started exhibiting lower cell viability than single-administrations after 24-hour cell incubation. After another 48 hours, the cell viability of co-administration dropped to 70%, while the cell viability of single-administrations remain the same as 24-hour incubation at 85-90%. At total concentration of 100 μ M, co-administration reached similar toxicity as single-administrations at 200 μ M after 72-hour incubation. The toxicity of dual-targeted MA was also examined on stromal cells (HS-5) and normal epithelial cells (Ect1/E6E7) (Figure S7B and S7C). **1** is biocompatible, while **2** shows certain toxicity on both cell lines. Without PLAP expression, both molecules target lysosomes of the cells (Figure S8). Co-administration exhibited median value toxicity of both single administrations being relatively biocompatible.

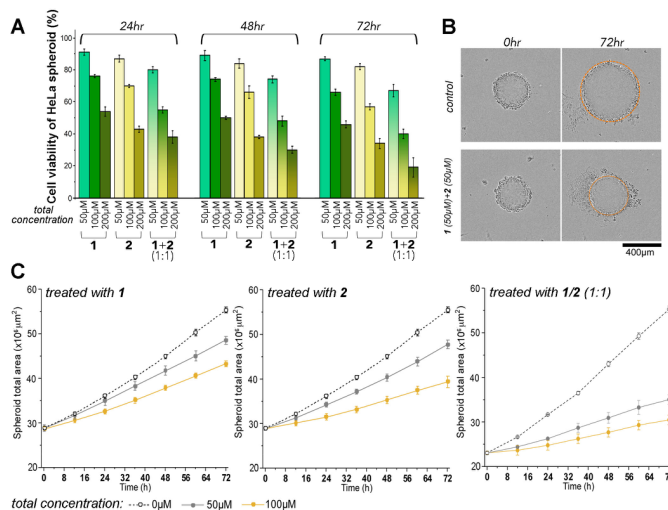


Figure 5. (A) HeLa cell over a 3-day period of incubation with **1**, **2** and mixture of **1** and **2** at 1:1 ratio at various concentrations in 3D cell culture. (B) Time-lapse optical images of HeLa spheroids with and without the treatment of **1** and **2** mixture at 1:1 ratio at total concentration of 100 μ M. (C) Time-dependent area size of HeLa cell spheroids incubated with **1**, **2** and mixture of **1** and **2** at 1:1 ratio at various concentrations.

Compared to the 90% closure rate of the control wound healing experiment, single-administration of **1** at 50 μ M and

100 μM concentrations resulted in 48% and 30% closure rates (Figure S7B and S8), while single-administration of **2** resulted in 40% and 20% closure rates, respectively (Figure S7B and S9). Co-administration at the same total concentrations led to 38% and 16% closure rates, respectively (Figure S7B and S10). Apparently, co-administration shows slightly higher inhibition efficacy than both single-administrations in 2D cell culture. In 3D cell culture, co-administration exhibited strong inhibition efficacy in the migration of HeLa spheroids (Figure 5B), superior to single-administrations. HeLa spheroids under the treatment of **1** at concentrations of 50 μM and 100 μM exhibit 87% and 78% of the total area of the control experiment after 72 hours, respectively (Figure 5C and S11). Under the treatment of **2** at the same concentrations, HeLa spheroids expand to 87% and 71% of the total area of the control experiment after 72 hours. Co-administration of **1** and **2** (1:1) at the same total concentrations resulted into spheroids with only 64% and 54% of the total area of the control experiment after 72 hours. Co-administration at total concentration of 50 μM showed higher inhibition efficacy on HeLa spheroid expansion than single-administrations at a concentration of 100 μM .

PLAP has been reported as tumor biomarker with elevated expression levels in tissues.²² PLAP expression of HeLa cells in different culture conditions was examined using imaging flow cytometry. In 3D cell culture, PLAP expression of HeLa cells is twice as high as in 2D cell culture (Figure S12). Since PLAP is essential in enzyme mediated dual-targeted MA, higher expression level may contribute to the greater anti-cancer efficacy of co-administration in 3D cell culture than in the 2D condition. Overall, greater anti-cancer efficacy of using **1** and **2** combinations for dual-targeted MAs compared with higher dose single molecule is identified on both cytotoxicity and migration inhibition of cervical cancer cells.

Conclusions

Enzyme-mediated plasma membrane and lysosome dual targeted MA introduces synergetic anti-cancer effect with amplified efficacy. It opens new opportunities in the application of nanotechnology for combination treatment. The differentiation of chiral molecules for divergent MA via enzyme-mediation in vitro also exhibits the advantages of using combinations of chiral peptides in drug design to avoid medication errors caused by drug-drug interactions.²³ Although the sequential engagement and mutual interactions are currently unclear, this research will contribute to comprehensive thought in protein interaction involved molecular assembly for advanced applications in cancer research.

Conflicts of interest

There are no conflicts to declare.

Acknowledgements

The research is supported by Okinawa Institute of Science and Technology Graduate University (OIST), Proof of Concept (POC) Program of OIST, and Takeda Science Foundation for medical science.

Notes and references

- 1 A. C. Lajoie, G. Lauziere, J. C. Lega, Y. Lacasse, S. Martin, S. Simard, S. Bonnett and S. Provencher, *Lancet Resp Med*, 2016, **4**, 291-305.
- 2 P. Rada, A. Mosquera, C. Garcia-Monzon, T. Iglesias and A. M. Valverde, *Diabetologia*, 2018, **61**, S61-S61.
- 3 J. J. Lu, W. Pan, Y. J. Hu and Y. T. Wang, *Plos One*, 2012, **7**.
- 4 I. M. Shaikh, K. B. Tan, A. Chaudhury, Y. J. Liu, B. J. Tan, B. M. J. Tan and G. N. C. Chiu, *J Control Release*, 2013, **172**, 852-861.
- 5 Y. Yuan, Z. Wang, P. Cai, J. Liu, L. D. Liao, M. Hong, X. Chen, N. Thakor and B. Liu, *Nanoscale*, 2015, **7**, 3067-3076.
- 6 Y. Kuang, J. F. Shi, J. Li, D. Yuan, K. A. Alberti, Q. B. Xu and B. Xu, *Angew Chem Int Edit*, 2014, **53**, 8104-8107.
- 7 G. Y. Li, T. Sasaki, S. Asahina, M. C. Roy, T. Mochizuki, K. Koizumi and Y. Zhang, *Chem*, 2017, **2**, 283-298.
- 8 T. Vanden Berghe, N. Vanlangenakker, E. Parthoens, W. Deckers, M. Devos, N. Festjens, C. J. Guerin, U. T. Brunk, W. Declercq and P. Vandenabeele, *Cell Death Differ*, 2010, **17**, 922-930.
- 9 L. Groth-Pedersen and M. Jaattela, *Cancer Lett*, 2013, **332**, 265-274.
- 10 A. C. Johansson, H. Appelqvist, C. Nilsson, K. Kagedal, K. Roberg and K. Ollinger, *Apoptosis*, 2010, **15**, 527-540.
- 11 S. Aits and M. Jaattela, *J Cell Sci*, 2013, **126**, 1905-1912.
- 12 A. Sano, E. Kakazu, T. Morosawa, J. Inoue, M. Ninomiya, T. Iwata, S. Takai, T. Nakamura, T. Shimosegawa and A. Masamune, *Hepatology*, 2018, **68**, 1015-1016.
- 13 P. H. Lange, J. L. Millan, T. Stigbrand, R. L. Vessella, E. Ruoslahti and W. H. Fishman, *Cancer Res*, 1982, **42**, 3244-3247.
- 14 S. Basak, I. Singh, A. Ferranco, J. Syed and H. B. Kraatz, *Angew Chem Int Edit*, 2017, **56**, 13288-13292.
- 15 H. Jedrzejewska and A. Szumna, *Chem Rev*, 2017, **117**, 4863-4899.
- 16 S. Guieu, J. Pinto, V. L. M. Silva, J. Rocha and A. M. S. Silva, *Eur J Org Chem*, 2015, 3423-3426.
- 17 S. Allenmark, *Chirality*, 2003, **15**, 409-422.
- 18 Y. Yang, Y. J. Zhang and Z. X. Wei, *Adv Mater*, 2013, **25**, 6039-6049.
- 19 J. Zhou, X. W. Du, C. Berciu, H. J. He, J. F. Shi, D. Nicastro and B. Xu, *Chem*, 2016, **1**.
- 20 D. R. McIlwain, T. Berger and T. W. Mak, *Csh Perspect Biol*, 2013, **5**.
- 21 J. Li, Y. Kuang, Y. Gao, X. Du, J. Shi and B. Xu, *J Am Chem Soc*, 2013, **135**, 542-545.
- 22 M. Orsaria, A. P. Londero, S. Marzinotto, C. Di Loreto, D. Marchesoni and L. Mariuzzi, *Cancer Biomark*, 2016, **17**, 479-486.
- 23 R. Ciraci, G. Tirone and F. Scaglione, *Pulm Pharmacol Ther*, 2014, **28**, 1-8.
- 24